Ceramics International **24** (1998) 507–513

PII: S0272-8842(97)00049-7
0272-8842/98 $19.00 + .00

Synthesis and Characterization of Ultrafine Lead Zirconate Powders

Jiye Fang,[a] John Wang,[a]* Ser-Choon Ng,[b] Leong-Ming Gan[c] & Chwee-Har Chew[c]

[a]Department of Materials Science, Faculty of Science, National University of Singapore, Singapore 119260
[b]Departments of Materials Science and Physics, Faculty of Science, National University of Singapore, Singapore 119260
[c]Departments of Materials Science and Chemistry, Faculty of Science, National University of Singapore, Singapore 119260

(Received 24 April 1997; accepted 27 May 1997)

Abstract: Ultrafine perovskite lead zirconate powders have been prepared via three types of processing routes: conventional solid reaction, conventional coprecipitations using either oxalic acid or ammonia solution as the precipitant, and microemulsion-refined coprecipitations using either oxalic acid or ammonia solution as the precipitant. The microemulsion-derived precursors exhibit a lower formation temperature for orthorhombic $PbZrO_3$ than the conventionally coprecipitated precursors. Ammonia solution appears to be a more attractive precipitant than oxalic acid in reducing the formation temperature for $PbZrO_3$. The microemulsion-derived lead zirconate powders, which are of dimension in the range of nanometers, are much finer in particle size and lower in particle agglomeration than the conventionally coprecipitated powders. © 1998 Elsevier Science Limited and Techna S.r.l.

1 INTRODUCTION

Lead zirconate has an orthorhombic structure at room temperature and transforms to cubic at around 230°C. It is an important end member of lead zirconate titanate (PZT) series and has been extensively studied because of its useful electro-optical[1–3] and piezoelectric properties.[4–8] Lead zirconate is also an important antiferroelectric material used in electronic devices such as capacitors.[9] Solid state reaction between PbO and ZrO_2 has often been used to prepare $PbZrO_3$ powders and sintered ceramics. Unfortunately, the completion of the solid reaction requires a considerably high temperature and the resulting powders exhibit many of the undesirable characteristics, such as a low chemical homogeneity, large particle size, wide particle size distribution and therefore low sinterability. Thus, a number of chemistry-based powder processing routes have recently been developed for the preparation of fine and homogeneous lead zirconia powders, including coprecipitation,[10–12] hydrothermal synthesis,[13–15] sol–gel techniques,[16–21] solution combustion[22,23] metalorganic chemical vapour deposition[24] and thermal decomposition.[25]

Several important ceramic powders have also been successfully prepared from water-in-oil microemulsions.[26–30] It has been shown that the microemulsion-derived ceramic powders are finer in particle size, narrower in particle size distribution, higher in sinterability, and more homogeneous in composition than many of those prepared via other processing routes. A microemulsion system, which consists of an oil phase, a surfactant phase and an aqueous phase, is a thermodynamically stable isotropic dispersion of the aqueous phase in the continuous oil phase.[27,31] The size of the aqueous droplets is in the range of 5 to 20 nm, rendering the microemulsion systems optically transparent. Chemical reactions, such as precipitation and co-precipitation, will take place when droplets containing the desirable reactants collide with each other. Each of these aqueous droplets in the two microemulsion systems will thus be acting as a nanosized reactor for forming nanosized precursor particles.

*To whom correspondence should be addressed; e-mail: maswangj@nus.sg

The objective of the present work is to synthesize and characterize ultrafine lead zirconate powders via microemulsion processing routes, and compare with those prepared via conventional solid reaction and coprecipitations. Two types of precipitant were used for both the conventional and microemulsion refined coprecipitations.

2 EXPERIMENTAL PROCEDURES

2.1 Starting materials

The starting materials used in the present work included: a high purity lead (II) nitrate (>99.7%), oxalic acid dehydrate (>99.9%), ammonium hydroxide (28.0–30.0%, all from J. T. Baker Inc., USA), a high purity zirconium oxynitrate solution (20 wt% ZrO_2, MEL, Manchester, UK), a high purity cyclohexane (AJAX Chemicals, Australia), lead oxide (>99.5%, Hayashi Pure Chemical Industries Ltd., Japan) and a mixed non-ionic surfactant consisting of poly (oxyethylene)$_5$ nonyl phenol ether (NP5) and poly (oxyethylene)$_9$ nonyl phenol ether (NP9) (weight ratio: 2:1, Albright and Wilson Asia Pte Ltd, Singapore).

2.2 Phase diagrams

The procedure of establishing a partial phase diagram at room temperature for the ternary system consisting of cyclohexane, NP5 + NP9 and an aqueous solution has been detailed elsewhere.[26–30] To locate the demarcation between the microemulsion and non-microemulsion regions, the aqueous phase was titrated into a mixture of given cyclohexane to surfactant ratio. Thorough mixing of the three components was achieved using a Vortex mixer. Microemulsion compositions appear optically transparent when the size of aqueous droplets is in the range of 5 to 20 nm, due to the fact that the nanosized aqueous droplets do not cause a substantial degree of light scattering. A series of such demarcation points were obtained by varying the cyclohexane to surfactant ratio. Partial phase diagrams at room temperature for three ternary systems were established. They consisted of cyclohexane, NP5 + NP9 and an aqueous phase containing 0.20 M $Pb(NO_3)_2$ + 0.24 M $ZrO(NO_3)_2$, 1.78 M ammonia and 0.67 M oxalic acid, respectively.

2.3 Preparation of $PbZrO_3$ powders

Five processing routes were used to prepare $PbZrO_3$, namely conventional solid reaction, conventional coprecipitations using either oxalic acid or ammonia solution as the precipitant; and microemulsion-refined coprecipitations using either oxalic acid or ammonia solution as the precipitant. The precursors and resulting $PbZrO_3$ powders derived from these five processing routes will be referred to as CSR, CCA, CCB, MRA and MRB, respectively.

In the conventional solid reaction route, lead oxide and zirconium oxide powders were mixed together by ball milling for 12 h in a mixture consisting of 60 wt% cyclohexane, 5 wt% NP5 + NP9 and 35 wt% deionized water. The suspension was then dried and subsequently calcined at various temperatures ranging from 700 to 900°C.

In the conventional coprecipitation routes, 100 ml of aqueous solution containing 22.8 mmol $Pb(NO_3)_2$ and 22.8 mmol $ZrO(NO_3)_2$ was titrated dropwise when vigorously stirred with 104 ml of 0.67 M oxalic acid ($H_2C_2O_4$) solution (CCA route). Similarly, the solution was titrated with 40 ml of 1.78 M ammonia solution in the CCB route. The resulting precipitates were washed repeatedly using de-ionized water and recovered by centrifugation, followed by drying first at 60°C and then at 140°C.

In the microemulsion-refined coprecipitation routes, three microemulsion compositions were prepared. They all consisted of 59.5 wt% cyclohexane, 25.5 wt% NP5/NP9 and 15.0 wt% aqueous phase. The aqueous phase contained either 0.20 M $Pb(NO_3)_2$ + 0.24 M $ZrO(NO_3)_2$, or 0.67 M $H_2C_2O_4$, or 1.78 M ammonia solution. Precursor MRA was prepared by reacting the microemulsion containing 15 wt% of 0.20 M $Pb(NO_3)_2$ + 0.24 M $ZrO(NO_3)_2$ with the one containing 0.67 M $H_2C_2O_4$. The reaction was brought about by mixing the two compositions together via vigorously stirring for more than 30 min. Similarly, precursor MRB was prepared by mixing the microemulsion containing 15 wt% of 0.20 M $Pb(NO_3)_2$ + 0.24 M $ZrO(NO_3)_2$ with the one containing 1.78 M ammonia solution. To retrieve the precipitates formed in microemulsions, the oil and surfactant were washed off using distilled ethanol, followed by recovery by centrifugation. They were dried first at 60°C and then at 140°C.

2.4 Powder characterizations

The as-dried precursors from the above five processing routes were characterized using thermogravimetric analysis (TGA) and differential thermal analysis (DTA) (Dupont Instruments) at a heating rate of 10°C per min in air from room temperature up to 900°C. They were then calcined in air at various temperatures, up to 900°C, followed by phase analysis using X-ray diffraction (CuKα, Philips

PW1729). Crystallite sizes in the calcined $PbZrO_3$ were estimated on the basis of line broadening at half maximum of the (221) peak. The calcined powders were also characterized for particle/agglomerate size distribution using laser light scattering technique (Horiba LA-910). BET surface analyser (Nova 2000, Quantachrome) and scanning electron microscope (JEOL, JSM-35CF) were employed to analyse the specific surface area, and particle/agglomerate morphology of these powders, respectively.

3 RESULTS AND DISCUSSION

Figure 1(a) shows the partial phase diagram established at room temperature for the ternary system consisting of cyclohexane, NP5 + NP9 and aqueous solution containing 0.20 M $Pb(NO_3)_2$ + 0.24 M $ZrO(NO_3)_2$. Similarly, the partial phase diagrams for those containing 0.67 M ($H_2C_2O_4$) and 1.78 M ammonia solution are shown in Fig. 1(b) and (c), respectively. In all three systems, the microemulsion region increases with increasing the ratio of (NP5 + NP9) to cyclohexane, although it is narrower in the system containing 1.78 M ammonia solution than in the other two. For example, the maximum loading of 0.20 M $Pb(NO_3)_2$ + 0.24 M $ZrO(NO_3)_2$ and 0.67 M $H_2C_2O_4$ in the microemulsion is up to ~30 wt% at a fixed cyclohexane to NP5 + NP9 weight ratio of 70:30, as compared to ~20 wt% for the 1.78 M ammonia solution.

Figure 2 shows the TGA and DTA traces at a heating rate of 10°C per min in air for precursors CCA, CCB, MRA and MRB, respectively. When oxalic acid is used as the precipitant, the precursors derived from the conventional coprecipitation and microemulsion-refined coprecipitation show similar weight loss steps with increasing temperature. A steady weight loss over the temperature range from room temperature to 300°C is followed by a fall in specimen weight at around 320°C. The steady weight loss over the low temperature range is due to the elimination of residual water and organic substance from these precursors. The fall in specimen weight over the high temperature range is related to the decomposition of Pb–Zr oxalate-hydrate. When 1.78 M ammonia solution is used as the precipitant, a considerable difference in weight loss with rising temperature is observed between the precursors derived from the above two processing routes. The precursor derived via the microemulsion-refined coprecipitation route does not show much weight loss with increasing temperature until 220°C, where a fall in specimen weight starts. In contrast, the precursor derived via the

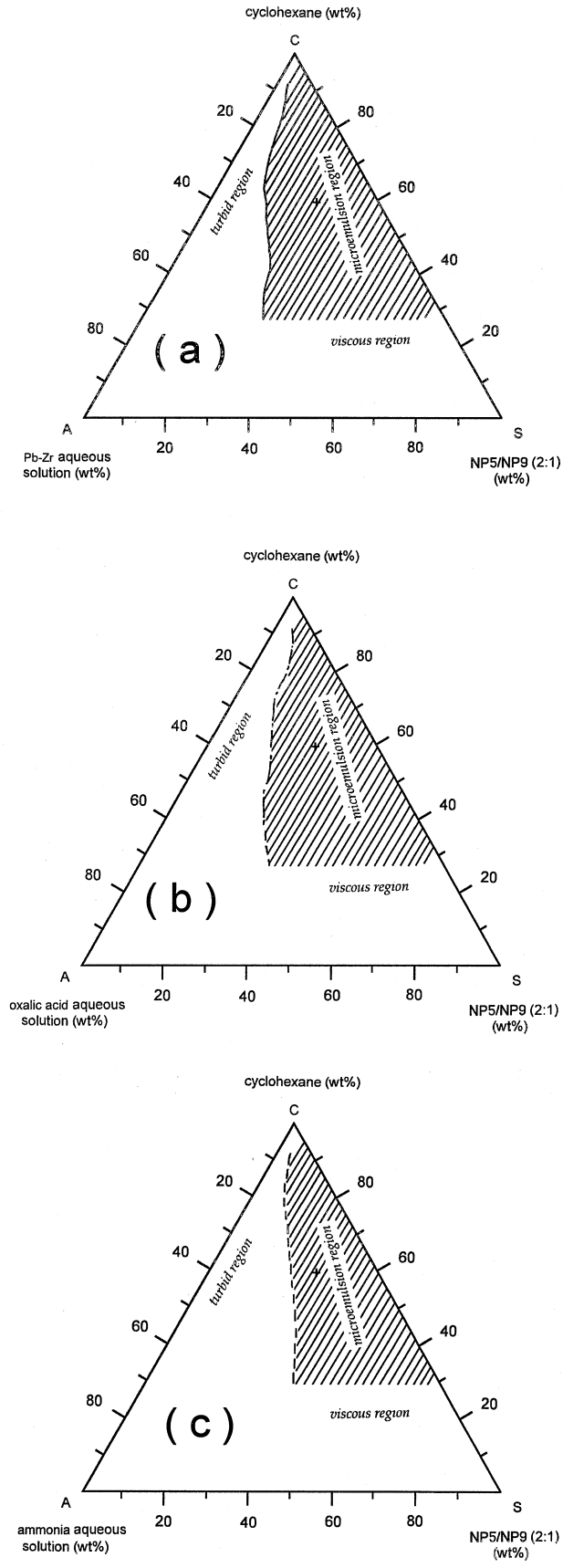

Fig. 1. Partial phase diagram established at room temperature for the ternary system consisting of cyclohexane, NP5 + NP9, and aqueous solution containing (a) 0.20 M $Pb(NO_3)_2$ + 0.24 M $ZrO(NO_3)_2$; (b) 0.67 M oxalic acid solution; (c) 1.78 M ammonia solution.

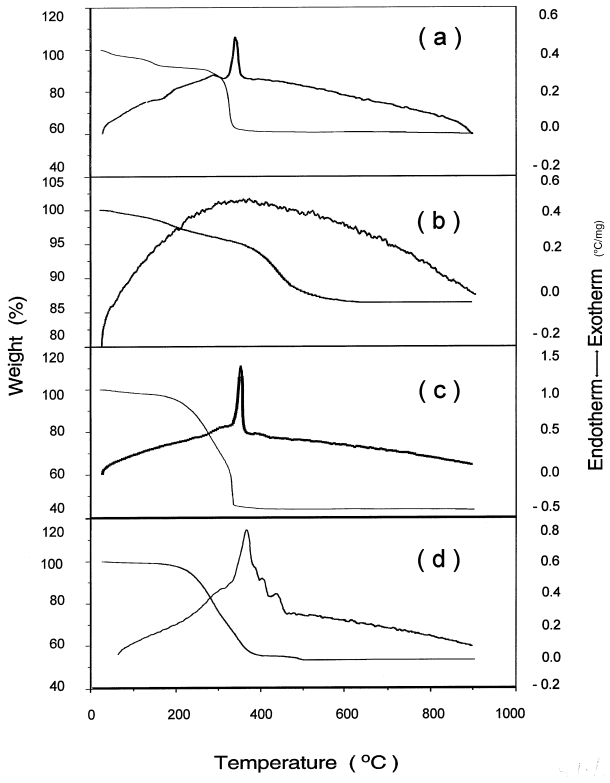

Fig. 2. TGA and DTA traces at a heating rate of 10°C per min in air for the precursors prepared via (a) conventional coprecipitation with oxalic acid solution as the precipitant, CCA; (b) conventional coprecipitation with ammonia solution as the precipitant, CCB; (c) microemulsion-refined coprecipitation with oxalic acid solution as the precipitant, MRA; and (d) microemulsion-refined coprecipitation with ammonia solution as the precipitant, MRB.

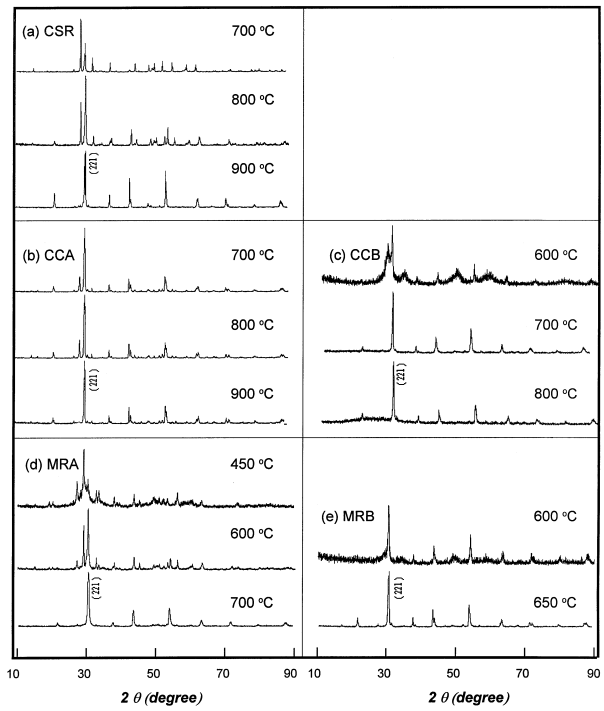

Fig. 3. XRD traces of the $PbZrO_3$ powders calcined for 1 hour at various temperatures and prepared via (a) the conventional solid processing route (CSR), (b) the conventional coprecipitation processing route with oxalic acid solution as the precipitant (CCA), (c) the conventional coprecipitation processing route with ammonia solution as the precipitant (CCB), (d) the microemulsion-refined coprecipitation processing route with oxalic acid solution as the precipitant (MRA), (e) the microemulsion-refined coprecipitation processing route with ammonia solution as the precipitant (MRB).

conventional coprecipitation route shows a slow weight loss over the wide temperature range from room temperature to 400°C, followed by a minor fall in specimen weight. Its completion temperature for weight loss (600°C) is higher than that in the former (500°C). Well defined exothermic peaks are observed for precursors CCA, MRA and MRB over the temperature range from 300 to 400°C. They occur at temperatures almost identical to those corresponding to the respective fall in specimen weight in the these precursors as shown in Fig. 2. This indicates that they are due to the decomposition of oxalate or hydroxide hydrates and the subsequent crystallization of lead and zirconium oxides. The absence of a well defined sharp exothermic peak in precursor CCB may be explained by a slow weight loss over the very wide temperature range from room temperature to 550°C.

To study the phase development with increasing calcination temperature in each of these precursors, they were calcined in air at various temperatures in the range from 400 to 1000°C. Calcination time was varied from 1 to 4 h at each temperature. Figure 3(a)–(e) the XRD traces for precursors CSR, CCA, CCB, MRA and MRB, respectively. They show considerably difference in the calcination temperature at which a high purity orthorhombic $PbZrO_3$ is obtainable. In the case of CSR, calcination at 700°C resulted in the formation of a small amount of orthorhombic $PbZrO_3$ in the mixed oxides. A calcination temperature of 900°C is required in order to develop a high purity orthorhombic $PbZrO_3$ phase. The precursor CCA derived via the conventional coprecipitation route using oxalic acid as the precipitant requires a similar calcination temperature for obtaining a predominant orthorhombic $PbZrO_3$ phase. In comparison, orthorhombic $PbZrO_3$ was the only detectable phase for the precursor CCB when calcined at 700°C for 1 h. Predominant orthorhombic $PbZrO_3$ phase is also obtainable in precursor MRA when it is calcined at 700°C, which is 200°C lower than that observed in precursor CCA. This indicates that the microemulsion refinement results in a lower formation temperature for orthorhombic $PbZrO_3$ when oxalic acid is used as the precipitant. But the precursor MRB derived via the microemulsion refined processing route with ammonia

solution as the precipitant shows the lowest formation temperature for orthorhombic $PbZrO_3$ as shown in Fig. 3(e).

A high purity orthorhombic $PbZrO_3$ phase is already developed when precursors MRB is calcined at 600°C, which is 100°C lower than that observed in the precursor MRA. The formation temperatures for orthorhombic $PbZrO_3$ observed in the precursors derived from microemulsions (especially with ammonia as the precipitant) are much lower than those reported for the precursors prepared via many other chemistry-based processing routes. For example, Jimenez and co-workers[12] coprecipitated an amorphous $PbZrO_3$ hydroxide precursor, which required a calcination at 800°C for forming a well-developed orthorhombic $PbZrO_3$ phase, although $PbZrO_3$ crystallites were observed to form at 700°C. The precursor synthesized by Li *et al.*[20] via a sol–gel processing route also requires a similar calcination temperature for forming the perovskite $PbZrO_3$ phase.

The average crystallite size in each of the calcined powders was calculated on the basis of line broadening of peak (221), using Scherrer equation.[32] Figure 4 shows the plots of the average crystallite size as a function of calcination temperature for samples CSR, CCA, CCB, MRA and MRB, respectively. As expected, they increase with increasing calcination temperature over the range from 600 to 1000°C. At each calcination temperature, MRA exhibits the smallest crystallite size, followed by MRB, CCB and CCA.

Calcined $PbZrO_3$ powders at 800°C for 1 h prepared via the CCA, CCB, MRA and MRB processing routes exhibit a BET specific surface area of 3.44, 6.14, 54.42 and 32.98 $m^2 g^{-1}$, respectively. The corresponding average particle size for these four powders is 219, 123, 14 and 23 nm, respectively. It is apparent that the two microemulsion-derived powders are much finer in discrete particle sizes than the two prepared via the conventional coprecipitation routes. In fact, specific surface areas of the latter two are comparable with that of CSR calcined at 900°C for 1 h (3.36 $m^2 g^{-1}$). The large difference in specific surface area between CCA and MRA and that between CCB and MRB demonstrates the effectiveness of microemulsion refinement in reducing the particle size of $PbZrO_3$ powders.

Figure 5 shows that the five $PbZrO_3$ powders also exhibit different particle size distributions when measured using laser light scattering technique. It was experimentally observed that the particle size distribution measured for each of these powders was dependent on how well the powder is dispersed in the liquid medium. For example, a longer ultrasonication stirring before measurement resulted in a better dispersion of the powder particles and thus a smaller particle size distribution. It is therefore believed that Fig. 5 represents the

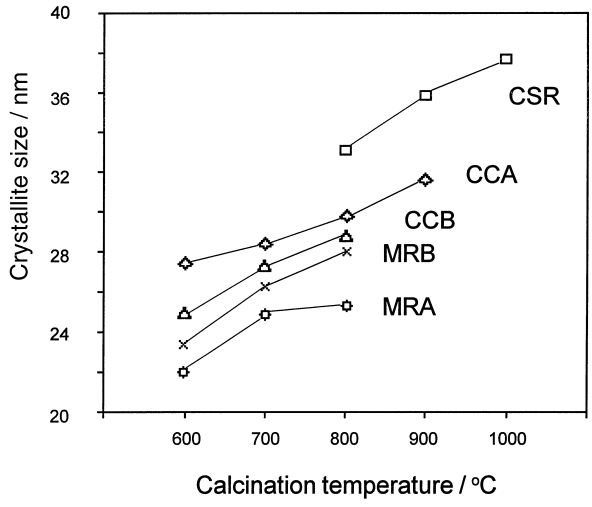

Fig. 4. The crystallite size of lead zirconate as a function of calcination temperature for the precursors derived via the CSR, CCA, CCB, MRA and MRB processing routes.

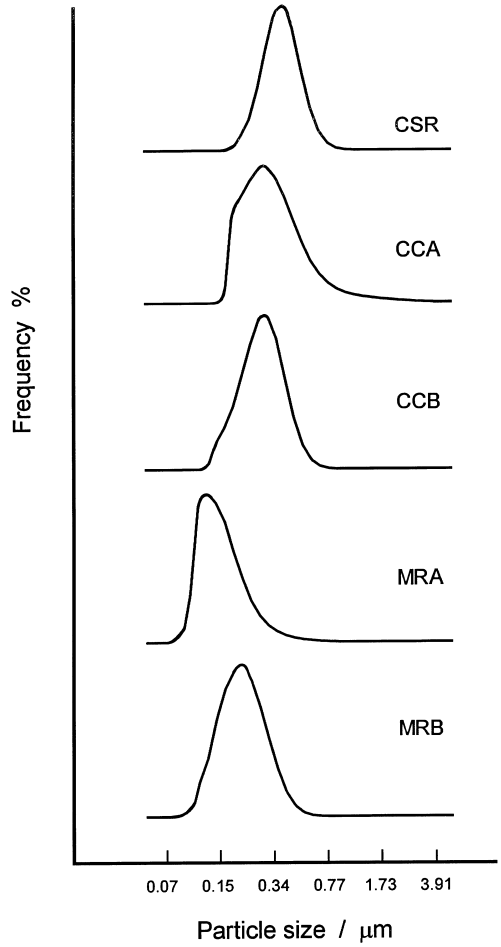

Fig. 5. The particle/agglomerate size distribution of $PbZrO_3$ powders derived via the CSR, CCA, CCB, MRA and MRB processing routes. CRS was calcined at 900°C for 1 h and the other four were calcined at 800°C for 1 h.

agglomerate size distributions in these powders, rather than their particle size distributions. These results were obtained after each powder was ultrasonically stirred for 14 min. In comparison, MRA covers the smallest size range from 0.08 to 0.6 μm, followed by MRB. The two conventionally precipitated powders are similar in particle/agglomerate size distribution. As expected, the conventionally reacted $PbZrO_3$ powder exhibits the largest particle/agglomerate size distribution, covering the size range from 0.2 to 1.3 μm. These particle/agglomerate size distributions are corroborated by the SEM micrographs shown in Fig. 6(a)–(e). Large particle agglomerates occur in CSR, CCA and CCB,

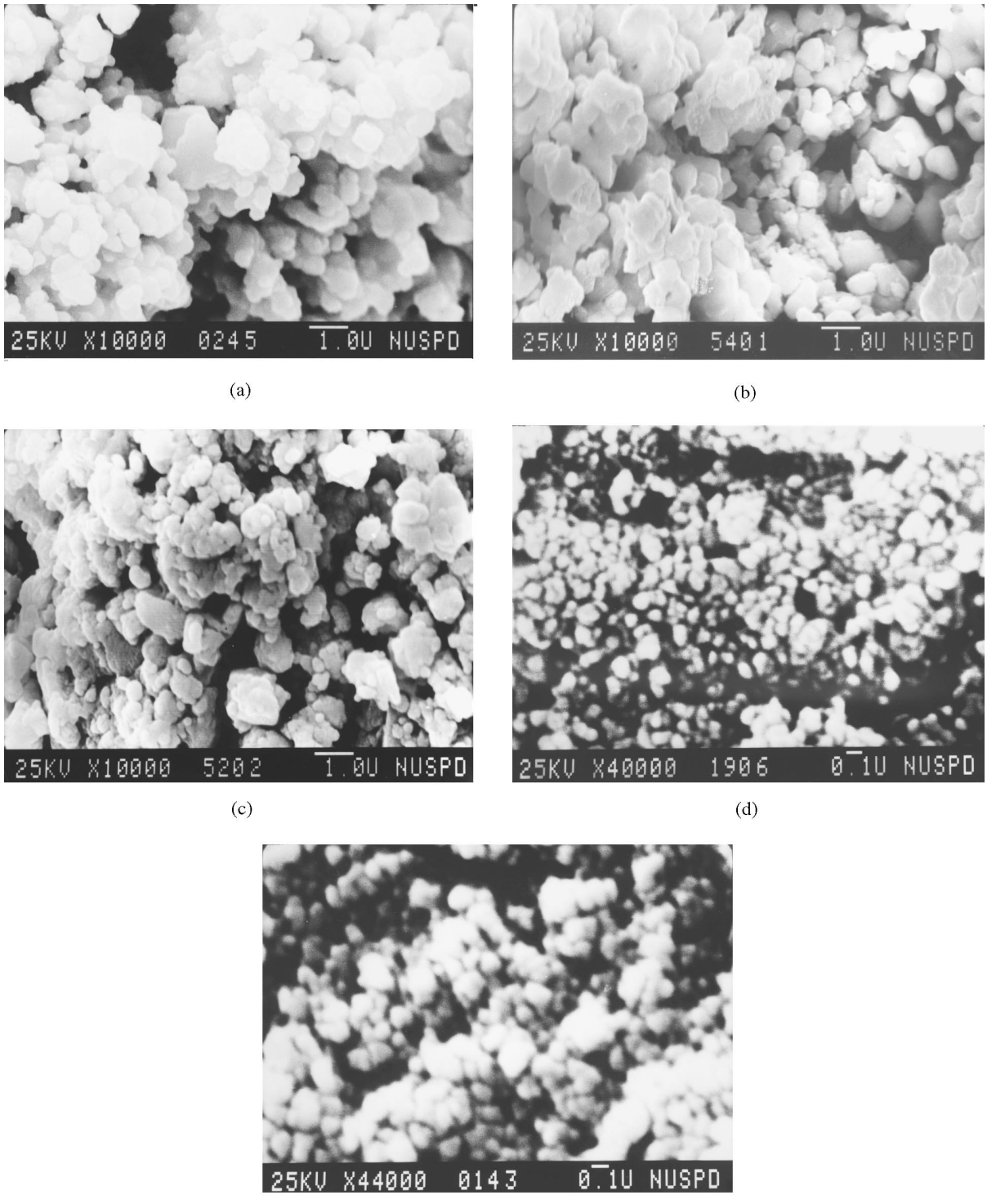

Fig. 6. SEM micrographs showing the $PbZrO_3$ powders prepared via (a) the conventional solid reaction, CSR; (b) conventional coprecipitation with oxalic acid solution as the precipitant, CCA; (c) conventional coprecipitation with ammonia solution as the precipitant, CCB; (d) microemulsion-refined coprecipitation with oxalic acid solution as the precipitant, MRA; and (e) microemulsion-refined coprecipitation with ammonia solution as the precipitant, MRB.

although the primary particles in these powders are in the range of 0.5 to 1.0 μm. In contrast, small (0.1 to 0.3 μm) and rather well dispersed $PbZrO_3$ particles occur in MRA and MRB. This demonstrates the great attractiveness of the microemulsion processing routes in preparing nanosized ceramic powders, when compared to the conventional coprecipitation routes.

4 CONCLUSIONS

Three types of processing routes have been used to prepare fine perovskite lead zirconate powders: conventional solid reaction, conventional coprecipitations using either oxalic acid or ammonia solution as the precipitant, and microemulsion-refined coprecipitation also using either oxalic acid or ammonia solution as the precipitant. The microemulsion-derived precursors exhibit a much lower formation temperature for orthorhombic $PbZrO_3$ phase than that in the conventionally coprecipitated precursors. Ammonia solution appears to be more attractive as a precipitant than oxalic acid in reducing the formation temperature for $PbZrO_3$. The microemulsion-derived lead zirconate powders, which are of dimension in the range of nanometers, are much finer in particle size and lower in particle agglomeration than the conventionally coprecipitated powders.

ACKNOWLEDGEMENT

This work was supported by research grants RP950613 and RP950605 from the National University of Singapore.

REFERENCES

1. HAERTLING, G. H., *Ferroelectrics*, **75** (1987) 25–55.
2. BRODY, P. S. (United States Dept. of the Army), US Patent No. 4 236 938, 2 December 1980.
3. PROKOPALO, O. I., FESENKO, E. G., MALITSKAYA, M. A., POPOV, Y. M. & SMOTRAKOV, V. G., *Ferroelectrics*, **18** (1978) 99–102.
4. GRIDNEV, S. A., PAVLOVA, N. G., GORBATENKO, V. V. & SHUVALOV, L. A., *Ferroelectrics*, **134** (1992) 365–369.
5. KAMATAKI, H., MATSUMOTO, T. & KAWAMURA, Y. (Fuji Electric Co., Ltd), Jpn Kokai Tokkyo Koho JP (Jpn Patent No.) 02,272,781 [90,272,781], 7 November 1990.
6. OVERSLUIZEN, T. & WATSON, G., *Nucl. Instrum. Methods Phys. Res. A*, **A246** (1986) 787–789.
7. YAMASHITA, Y., TOSHIDA, S., HARADA, M. & TAKAHASHI, T. (Toshiba Corp.), Jpn Kokai Tokkyo Koho JP (Jpn Patent No.) 61,129,888 [86,129,888], 17 June 1986.
8. JAFFE, B., COOK, W. R. & JAFFE, H., *Piezoelectric Ceramics*. Academic Press, London, 1971, pp. 123–131.
9. SONY CORP., Eur. Pat. Appl. EP 200,176, 10 December 1986.
10. TAKAHASHI, K., ODA, M. & SHIBATANI, H. (Mitsubishi Petrochemical Co., Ltd), Jpn Kokai Tokkyo Koho JP (Jpn Patent No.) 62,72,524 [87,72,524], 3 April 1987.
11. SAEKI, K. & SHIRASAKI, S. (Nippondenso Co., Ltd; National Institute forResearch in Inorganic Materials), Jpn Kokai Tokkyo Koho JP (Jpn Patent No.) 63,151,671 [88,151,671], 17 December 1986.
12. JIMENEZ, C. M., ARROYO, G. F. & GUILLEN, L. D. O., In *Ceramic Powders*, ed. P. Vincenzini. Elsevier Scientific, Amsterdam, 1983, pp. 565–574.
13. CHENG, H., MA, J., ZHU, B. & CUI, Y., *J. Am. Ceram. Soc.*, **76** (1993) 625–629.
14. LIN, C. H., PEI, S. C., CHIN, T. S. & WU, T. P., *Ceram. Trans.*, **32** (1993) 261–274.
15. WATANABE, M., SHIMIZU, Y. & HATA, H. (Osaka Titanium Co., Ltd), Jpn Kokai Tokkyo Koho JP (Jpn Patent No.) 03,122,021 [91,122,021], 24 May 1991.
16. SENGUPTA, S. S., MA, L., ADLER, D. L. & PAYNE, D. A., *J. Mater. Res.*, **10** (1995) 1345–1348.
17. WILKINSON, A. P., SPECK, J. S., CHEETHAM, A. K., NATARAJAN, S. & THOMAS, J. M., *Chem. Mater.*, **6** (1994) 750–754.
18. TEOWEE, G., BOULTON, J. M., MOTAKEF, S., UHLMANN, D. R., ZELINSKI, B. J. J., ZANONI, R. & MOON, M., *Proc. SPIE-Int. Soc. Opt. Eng.*, **1758** (Sol–gel Opt. II) (1992) 236–248.
19. FAURE, S. P., BARBOUX, P. & GANNE, J. P., *Ferroelectrics*, **128** (1992) 19–24.
20. LI, S., CONDRATE, R. A., JANG, S. D. & SPRIGGS, R. M., *J. Mater. Sci.*, **24** (1989) 3873–3877.
21. BUDD, K. D., DEY, S. K. & PAYNE, D. A., *Brit. Ceram. Proc.*, **36** (1985) 107–112.
22. SEKAR, M. M. A. & PATIL, K. C., *J. Mater. Chem.*, **2** (1992) 739–743 (and 1215 (correction)).
23. KINGSLEY, J. J., MANICKAM, N. & PATIL, K. C., *Bull. Mater. Sci.*, **13** (1990) 179–183.
24. BAI, G. R., CHANG, H. L. M., LAM, D. J. & GAO, Y., *Appl. Phys. Lett.*, **62** (1993) 1754–1756.
25. SAIKALI, Y., ROUBIN, M. & DURAND, B., *Ann. Chim.*, **17** (1992) 123–130.
26. FANG, J., WANG, J., NG, S.-C., CHEW, C.-H. & GAN, L.-M., submitted for publication in *J. Mater. Sci.*
27. FANG, J., WANG, J., NG, S.-C., CHEW, C.-H. & GAN, L.-M., *Nanostruct. Mater.*, **8** (1997) 499–505.
28. GAN, L. M., ZHANG, L. H., CHAN, H. S. O., CHEW, C. H. & LOO, B. H., *J. Mater. Sci.*, **31** (1996) 1071–1079.
29. LIM, G. K., WANG, J. NG S. C. & GAN, L. M., *Mater. Lett.*, **28** (1996) 431–436.
30. GAN, L. M., CHAN, H. S. O., ZHANG, L. H., CHEW, C. H. & LOO, B. H., *Mater. Chem. Phys.*, **37** (1994) 263–268.
31. CHIENG, T. H., GAN, L. M., CHEW, C. H. and NG, S. C., *Polymer*, **36** (1995) 1941–1946.
32. KLUG, H. P. & ALEXANDER, L. E., *X-Ray Diffraction Procedures for Polycrystalline and Amorphous Materials*. Wiley, New York, 1954, pp. 491–538.